Nat Cell Biol. Author manuscript; available in PMC 2019 January 30.

Published in final edited form as:
Nat Cell Biol. 2018 September ; 20(9): 1032–1042. doi:10.1038/s41556-018-0155-7.

Scale-invariant patterning by size-dependent inhibition of Nodal signalling

María Almuedo-Castillo[1,†], **Alexander Bläßle**[1], **David Mörsdorf**[1], **Luciano Marcon**[1,†], **Gary H. Soh**[1], **Katherine W. Rogers**[1,2], **Alexander F. Schier**[2], and **Patrick Müller**[1,*]

[1]Friedrich Miescher Laboratory of the Max Planck Society, Max-Planck-Ring 9, 72076 Tübingen (Germany)

[2]Department of Molecular and Cellular Biology, Harvard University, 16 Divinity Avenue, Cambridge, MA 02138 (USA)

Abstract

Individuals can vary significantly in size, but the proportions of their body plans are often maintained. We generated smaller zebrafish by removing 30% of their cells at blastula stages and found that these embryos developed into normally patterned individuals. Strikingly, the proportions of all germ layers adjusted to the new embryo size within two hours after cell removal. Since Nodal/Lefty signalling controls germ layer patterning, we performed a computational screen for scale-invariant models of this activator/inhibitor system. This analysis predicted that the concentration of the highly diffusive inhibitor Lefty increases in smaller embryos, leading to a decreased Nodal activity range and contracted germ layer dimensions. *In vivo* studies confirmed that Lefty concentration increased in smaller embryos, and embryos with reduced Lefty levels or with diffusion-hindered Lefty failed to scale their tissue proportions. These results reveal that size-dependent inhibition of Nodal signalling allows scale-invariant patterning.

Introduction

Despite often significant variability in size, embryos faithfully generate the correct tissue proportions1–5. During development, tissue patterning is achieved by gradients of signalling proteins that induce distinct differentiation programs in discrete spatial domains6–10. To

*Correspondence should be addressed to P.M.
†Present address: Centro Andaluz de Biología del Desarrollo, Universidad Pablo de Olavide, Carretera de Utrera km1, 41013 Sevilla (Spain)

Author Contributions

M.A.C, A.F.S., and P.M. conceived the study; P.M. developed the extirpation assay and supervised the project; G.H.S developed the extirpation device and the 2D map visualisation workflow, and optimised the pSmad2/3 immunostaining protocol; D.M. performed the experiments in Fig. 6i,j, Supplementary Fig. 4f,g, Supplementary Fig. 5, and Supplementary Fig. 8, and contributed to experiments in Fig. 6f,h; K.W.R. and A.F.S. contributed the data in Supplementary Fig. 3d,e and provided the *lefty* mutants before publication; M.A.C. performed all other experiments; M.A.C., A.B., D.M., and P.M. analysed the data; A.F.S. and P.M. conceptualised the scaling model; A.B. performed the mathematical analysis and simulations with assistance from L.M. and P.M.; M.A.C. and P.M. wrote the manuscript with input from all authors.

Competing Interests

The authors have no competing interests.

adjust tissue patterning and organ proportions to their body size, embryos need to appropriately scale the underlying signalling gradients11. Scaling mechanisms for individual tissue-specific signalling systems at different stages of development have been proposed, but how these mechanisms are integrated and coordinated during development to generate the correct proportions of all tissues is currently unclear11–21. Here, we analysed how signalling gradients adjust tissue proportions in differently sized zebrafish embryos and identified a size-dependent mechanism that mediates scale-invariant germ layer patterning to provide the correct amount of progenitor cells for all future tissues.

Results

Scaling of tissue proportions in differently sized zebrafish embryos

We found that removal of ≈30% of cells by extirpation from the animal pole before gastrulation (Fig. 1a) generates zebrafish embryos that become normally patterned adults. Extirpated embryos developed into smaller individuals with the same number of proportionally thinner somites as untreated embryos (Fig. 1a). Consistently, the size of various organs including hatching gland (a mesodermal derivative, *hgg1*-positive) and eye (an ectodermal derivative, *vsx2*-positive) was reduced in individuals developing from extirpated embryos (Fig. 1b). Strikingly, scaling of tissue proportions to embryo size already occurred during gastrulation stages within 2 hours following extirpation. Using *in situ* hybridisation, we quantified the extent of presumptive ectoderm (*sox3*-positive, Fig. 1c) and mesendoderm (*fascin*-positive, Fig. 1d) and found that germ layer proportions adjusted progressively after extirpation: At 1 hour post extirpation (hpe), extirpated embryos had excess mesendoderm and insufficient ectodermal progenitors since cells were removed from the animal pole containing presumptive ectoderm (Fig. 1c,d). Interestingly, 1 hour later (2 hpe) ectoderm and mesendoderm proportions had adjusted in extirpated embryos (Fig. 1c,d). Using *in toto* light-sheet imaging, we confirmed that mesendoderm scaled throughout the embryonic marginal zone (Fig. 1e-g). Even though cells were removed from the animal pole, the number of endodermal precursor cells (*sox17*- and *sox32*-positive) at the opposite side within the marginal zone of extirpated embryos was also proportionally reduced by gastrulation stages (Fig. 1h).

Smaller embryos do not adjust developmental speed after extirpation

Cell density did not change (Fig. 2a) and proliferation rates did not increase in extirpated embryos (Fig. 2b,c), indicating that neither changes in cell density nor compensatory proliferation underlie germ layer scaling. Moreover, the spatial expression kinetics of *goosecoid*22 – a highly sensitive indicator of developmental progression – were similar in untreated and extirpated embryos at different developmental time points (Supplementary Fig. 1). Even though smaller embryos displayed a reduced apparent epiboly due to the shortened blastoderm but unchanged yolk extent after extirpation, the spreading of the blastoderm during epiboly occurred at a similar pace (Fig. 2d-i). Thus, scaling can also not be explained by altered developmental speed in differently sized embryos.

Nodal signalling scales in smaller embryos

Since the Nodal/Lefty activator/inhibitor system patterns the germ layers during early development10, 23, we hypothesised that Nodal signalling adjusts in smaller embryos to allow proportionate patterning. The activator Nodal is secreted from the marginal zone of the embryo and induces endoderm and mesoderm, whereas the highly diffusive Nodal inhibitor Lefty24, which is also expressed at the margin and induced by Nodal signalling, limits the mesendodermal domain23, 25–34. To test whether Nodal signalling adjusts in smaller embryos, we measured the extent of Nodal activity by assessing the phosphorylation of the Nodal signal transducer Smad2/323, 35, 36, pSmad2/3 (Fig. 3a-d, Supplementary Fig. 2a,b). Similar to the mesendodermal domain (Fig. 1e,f), Nodal signalling scaled throughout the embryonic marginal zone by 2 hpe (Fig. 3b,c). Interestingly, Nodal signalling already scaled by 1 hpe (Fig. 3a, Supplementary Fig. 2a,b), preceding the scaling of presumptive ectoderm/mesendoderm (Fig. 1c,d) and feedback-induced Nodals (*cyclops* and *squint*) and Leftys (*lefty1* and *lefty2*) (Fig. 3e-i).

A computational screen to identify scaling mechanisms

To identify the mechanism by which Nodal signalling might sense embryo size and adjust tissue proportions, we performed a computational screen including known positive and negative interactions in the Nodal/Lefty system23, 33, 34 while keeping model complexity to a minimum (Fig. 4a,b, Supplementary Note 1). We constrained the screen with the measured biophysical properties, including Nodal/Lefty diffusivities and half-lives33, and systematically varied the unknown parameters to identify systems that recapitulate the scaling observed during germ layer patterning. To keep model complexity minimal, we did not account for spatial biases influencing the Nodal/Lefty system37 and did not explicitly model receptor interactions38.

We screened more than 400,000 parameter combinations representing the production of Lefty, the inhibition strength, and the Nodal-mediated feedback on Nodal and Lefty production. By assessing the overlap between Nodal signalling in simulations of normally sized and shortened embryos, we found that systems capable of scaling require precise levels of highly diffusive Lefty, whose concentration increases in extirpated embryos to adjust the Nodal signalling gradient (Fig. 4c-e). In such systems, the boundary located more proximal to the marginal zone in shortened compared to normally sized embryos affects the long-range Lefty but not the short-range Nodal gradient (Fig. 4c). Since we shortened embryos prior to the onset of Lefty protein secretion without removing *Lefty*-expressing cells from the marginal zone (Fig. 3e-i), the same amount of Lefty should be produced in early extirpated and untreated embryos. Therefore, the concentration of Lefty should increase in smaller embryos, contracting the Nodal activity range to re-establish the correct tissue dimensions relative to the new size of the embryo.

In our simulations of the Nodal/Lefty system (Supplementary Movie 1), scale-invariant germ layer patterning only became apparent around 2 hpe, as observed experimentally (Fig. 1c,d). The simulations further closely matched the time window of germ layer specification: Nodal signalling levels and mesendoderm specification expand as development proceeds, Nodal signalling levels peak around 2 hpe (6 hours post fertilisation), and Nodal signalling rapidly

decreases afterwards (Supplementary Movie 1). Together, the experimental observations and computational simulations suggest that germ layer scaling at 2 hpe results from adjustments in mesendoderm expansion dynamics over time rather than from shrinking an initially too broadly specified mesendodermal domain.

Scaling depends on Lefty levels

Our model predicted that scaling crucially depends on the levels of Lefty (Fig. 4d, Fig. 5a,b). To test this prediction, we assessed mesendoderm proportions in embryos with varying numbers of functional *lefty* alleles (*lefty1* and *lefty2*)36. As expected, both untreated and extirpated double-homozygous *lefty1*$^{-/-}$;*lefty2*$^{-/-}$ mutants showed dramatically increased Nodal signalling and expanded mesendoderm36 (Fig. 5c-g, Supplementary Fig. 3a-c). In contrast, untreated and shortened double-heterozygous *lefty1*$^{+/-}$;*lefty2*$^{+/-}$ embryos exhibited nearly normal Nodal signalling and mesendoderm and ectoderm proportions, indicating that one functional allele of each *lefty* is sufficient for proper spatial Nodal signalling and scaling, possibly due to dosage adjustments that result in similar amounts of protein (Fig. 5c-h, Supplementary Fig. 3a-c). Normally sized and extirpated single-homozygous *lefty2*$^{-/-}$ mutants had excess Nodal signalling and mesendoderm at the expense of ectoderm (Fig. 5c-h, Supplementary Fig. 3a-c). In striking contrast, single-homozygous *lefty1*$^{-/-}$ embryos displayed expanded Nodal signalling and mesendoderm and reduced ectoderm only after extirpation (Fig. 5c-h, Supplementary Fig. 3a-c). Interestingly, Lefty1 is less inhibitory than its paralog Lefty2 (Supplementary Fig. 3d,e); thus, while highly active Lefty2 is sufficient for germ layer patterning in normally sized embryos, the correct levels of less active Lefty1 are required for scale-invariant patterning in significantly smaller embryos. These experimental findings support the simulations of our size-dependent inhibition model (Fig. 4d, Fig. 5a,b), showing that a small reduction in Lefty production, which does not significantly affect mesendoderm formation, abrogates scaling.

Scaling depends on highly diffusive Lefty

The second prediction of our model is that scaling depends on the high diffusivity of Lefty, which must reach the end of the patterning field (Fig. 4e, Fig. 6a,b). To test this prediction, we decreased Lefty diffusivity and determined the consequences on scaling. To obtain a patterning system in which the diffusion of Lefty1 can be experimentally manipulated, we first generated embryos in which the only source of Lefty was Lefty1-GFP. We rescued *lefty1*$^{-/-}$;*lefty2*$^{-/-}$ double mutants by injecting highly precise and physiologically relevant amounts (see Methods for details) of *lefty1-GFP* mRNA into the yolk syncytial layer (YSL) to mimic the secretion of endogenous Lefty from the marginal zone (Fig. 6c). Consistent with the high diffusivity of Lefty33, 39, Lefty1-GFP reached the end of the patterning field within 60 min after YSL injection (Fig. 6d,e, Supplementary Movie 2). A large proportion of *lefty1*$^{-/-}$;*lefty2*$^{-/-}$ mutant embryos was rescued to adulthood with this method in normally sized (≈70% fully or partially rescued) and extirpated (≈60% fully or partially rescued) embryos (Fig. 6f-h, Supplementary Fig. 4a-d). Thus, Lefty1-GFP provided from the marginal zone is sufficient not only to pattern germ layers but also to allow scaling. Next, to hinder Lefty1-GFP diffusion we used a “morphotrap” – an mCherry-labeled membrane-localised GFP-binding nanobody40. Co-injection of mRNA encoding the morphotrap and *lefty1-GFP* mRNA into one-cell stage embryos changed the localisation of Lefty1-GFP from

uniform extracellular to strongly membrane-associated (Supplementary Fig. 4e). Crucially, the diffusion coefficient of Lefty1-GFP in embryos expressing the morphotrap was significantly lower (D = 7.7 ± 3.2 (SD) μm^2/s for Lefty1-GFP, and 0.2 ± 0.2 (SD) μm^2/s for Lefty1-GFP + morphotrap; Fig. 6i,j). In addition, the activity of Lefty was decreased by morphotrap binding (Supplementary Fig. 4f,g).

We then injected mRNA encoding the morphotrap into *lefty1*$^{-/-}$;*lefty2*$^{-/-}$ mutant embryos at the one-cell stage and generated local sources of Lefty1-GFP at the marginal zone (Fig. 6d,e). The expression of the morphotrap dramatically changed the range of Lefty1-GFP from a nearly uniform distribution to a short-range gradient that did not reach the end of the embryo (Fig. 6d,e, Supplementary Movie 2, Supplementary Movie 3). In normally sized embryos, hindered Lefty diffusion did not significantly affect germ layer patterning (Fig. 6f-h), possibly due to decreased Lefty activity in the presence of morphotrap (Supplementary Fig. 4f,g). The change in Lefty distribution correlated with a steep drop in the rescue of extirpated embryos (Fig. 6f,g) and with expanded mesendoderm (Fig. 6h, Supplementary Fig. 4c,d). Simulations of the size-dependent inhibition model with hindered Lefty diffusion recapitulated the experimentally observed change in Lefty distribution (Fig. 6a,b,d,e): The decreased Lefty range precludes scaling of Nodal signalling since Lefty cannot reach the distal end of the patterning field. Together, these observations show that hindering Lefty diffusion prevents scaling in extirpated embryos, supporting the prediction of the size-dependent inhibition model.

Lefty concentration increases in smaller embryos

The third prediction of our model is that inhibitor concentration increases to reduce Nodal signalling in extirpated embryos (Fig. 4c, Fig. 7a), whereas the total amount of Lefty should slightly decrease over time due to feedback regulation (Fig. 7b). To test this prediction, we used quantitative immunoblotting and measured the amount of endogenous Lefty1 and Histone H3 as a proxy for cellular mass. Histone H3 levels were reduced by approximately one third after extirpation (Supplementary Fig. 5a-c). Importantly, Histone H3 signal intensity increased proportionally when 5, 10, or 15 embryos were loaded, showing that changes in total protein can be detected reliably (Supplementary Fig. 5c). The decrease in Lefty1 amounts in extirpated embryos was less pronounced compared to Histone H3 levels, resulting in increased Lefty1 concentration as predicted by the model (Supplementary Fig. 5b). However, Lefty1 intensities detected by the only currently available antibody against a zebrafish Lefty35 were low (Supplementary Fig. 5a, see Supplementary Fig. 8 for unprocessed data); sufficient Lefty1 levels could only be reliably detected after 50% epiboly stages, so that earlier dynamics of potential changes in Lefty1 levels could not be analysed. To corroborate these findings and to uncouple the rise in Lefty concentration from feedback regulation, we quantified GFP intensity after injection of physiologically relevant amounts of *lefty1-GFP* mRNA in the YSL and found that extirpated embryos exhibited higher GFP intensity than normally sized embryos (Fig. 7c).

Exogenous inhibitor can mediate scaling in lieu of Lefty

To assess whether this increase in inhibitor concentration is required for germ layer scaling, we analysed mesendoderm patterning in untreated and extirpated *lefty1*$^{-/-}$;*lefty2*$^{-/-}$ mutants

upon exposure to the small-molecule Nodal inhibitor SB-50512436. In contrast to the YSL-injection rescue approach, a reduction in embryo size should not affect the concentration of the tonic Nodal inhibitor in this experimental setup (Supplementary Fig. 6a-d). A large fraction of untreated *lefty1*$^{-/-}$;*lefty2*$^{-/-}$ mutants (≈90%, Fig. 7d,e) was rescued by 4.8 μM of Nodal inhibitor exposure. In contrast, exposure of extirpated *lefty1*$^{-/-}$;*lefty2*$^{-/-}$ mutants to the same inhibitor concentration resulted in abnormal mesendoderm proportions, and only ≈30% displayed some phenotypic rescue (Fig. 7d,e, Supplementary Fig. 6e,f). These results show that tonic size-independent inhibition levels effective in normally sized embryos do not allow scaling, since inhibitor concentration cannot increase in shortened embryos.

Our model implies that increasing tonic Nodal inhibitor levels should restore the appropriate Nodal signalling range in extirpated embryos. Consistent with this prediction, increasing the exposure of the small-molecule Nodal inhibitor from 4.8 μM to 6-7 μM significantly improved the rescue of extirpated *lefty1*$^{-/-}$;*lefty2*$^{-/-}$ mutants from ≈26% to ≈64% (Fig. 7e, Supplementary Fig. 6g), demonstrating that increased inhibitor levels are required for scaling in extirpated embryos.

Discussion

Together, four lines of evidence suggest that scale-invariant germ layer patterning is achieved by size-dependent inhibition of Nodal signalling. First, reduction of Lefty levels (Fig. 5) precludes scaling. Second, decreasing Lefty diffusivity interferes with scale-invariant patterning (Fig. 6). Third, the concentration of the Nodal inhibitor Lefty increases in extirpated embryos (Fig. 7c, Supplementary Fig. 5b). Fourth, rescue of extirpated *lefty1*$^{-/-}$;*lefty2*$^{-/-}$ mutants requires higher amounts of Nodal inhibitor drug than non-extirpated mutants (Fig. 7e, Supplementary Fig. 6g). In agreement with our mathematical model (Fig. 4, Supplementary Fig. 7, Supplementary Note 1), these results support the idea that the concentration and high diffusivity of Lefty are essential to adjust germ layer proportions.

The initial computational screen used *fascin* as a proxy for mesendoderm formation, which in addition to Nodal is also under the control of FGF signalling10, 35. For the simplified screening model we subsumed the action of Nodal and FGF into one effective signalling gradient, since the induction of *FGF* and *fascin* both depend on Nodal signalling35, 41–44, Nodal and FGF signals have similar effective mobilities in zebrafish embryos33, 39, and the range of *fascin* can be changed by Lefty-dependent modulation of Nodal signalling32, 33. Our conclusions are therefore not affected by how FGF, acting downstream of Nodal signalling, helps regulate *fascin* expression together with Nodal. In more refined simulations, we demonstrate the plausibility of our model for Nodal signalling based on pSmad2/3 activity (Supplementary Fig. 7m,n), a direct readout of Nodal activity. While tissue proportions might be further refined by interactions with other signalling pathways such as BMP and FGF10, 35, 43, 45 (Supplementary Fig. 7o,p, Supplementary Note 1), the scaled distribution of the Nodal signal transducer pSmad2 – which is independent of BMP and FGF – and the scaled tissue proportions in *lefty* mutants rescued by feedback-uncoupled Lefty – in which Lefty production is not under any transcriptional regulation – demonstrate the central role of Lefty in germ layer scaling.

In agreement with previous findings10, 36, 46, 47 our results suggest that Nodal-mediated germ layer patterning is robust to variations in signalling. Although mesendoderm is significantly expanded in *lefty1*$^{-/-}$ extirpated and *lefty2*$^{-/-}$ untreated embryos (Supplementary Fig. 3c), most of them develop with normal morphology (Fig. 5, Supplementary Fig. 3b). This suggests that embryos can adapt to a certain degree of mesendoderm expansion, possibly up to ≈42% (Supplementary Fig. 3a-c). However, this margin of tolerance is reduced in *lefty1*$^{-/-}$;*lefty2*$^{-/-}$ embryos rescued with YSL-expressed Lefty1-GFP, and an increase in the mesendoderm domain above ≈35% in this context appears to invariably prevent phenotypic rescue. Patterning robustness might therefore arise from Nodal/Lefty regulatory feedback, which is absent in *lefty1*$^{-/-}$;*lefty2*$^{-/-}$ mutant embryos but present in embryos with at least one intact Lefty paralog.

Previously postulated feedback-dependent scaling systems rely on modulators whose concentrations change depending on tissue size to adjust signalling activity range by modulating the signal's diffusion or clearance11, 14, 48–56. The Nodal/Lefty activator/inhibitor system is an excellent candidate for a modulator-based scaling mechanism: i) Lefty (modulator) inhibits Nodal activity by binding and preventing it from activating its receptors, ii) Nodal activity range is unaffected by the size reduction in extirpated embryos since the Nodal distribution is restricted to the marginal zone due to its low diffusivity33, iii) Lefty diffuses significantly faster than Nodal and exhibits a nearly uniform distribution33, 36 (Fig. 4c, Fig. 6d,e,i, Supplementary Movie 2), and iv) the production of Lefty is independent of the changes in size since Lefty-producing cells are located at the margin, which remains unaffected immediately following extirpation (Fig. 3e-i). An example of a modulator-based scaling mechanism is the recently proposed “expansion-repression” model, in which scaling of signalling gradients is achieved by an expander that increases the signal's range and that is itself repressed by the signal51. Superficially, our model can be interpreted as a mirror image of the “expansion-repression” model – i.e. a “contraction-activation” system – since the “inhibitor” or “contractor” Lefty restricts the signal's (Nodal) range and is activated by the signal. However, our theoretical model does not depend on feedback between signal and modulator. Since in our system the modulator inhibits the signal, it is sufficient to couple the changes in the concentration of the inhibitor to size in order to confer proportionate patterning. Similarly, we showed experimentally that Nodal-mediated Lefty activation is dispensable for scaling (Fig. 6, Fig. 7, Supplementary Fig. 4, Supplementary Fig. 6). This suggests that scale-invariant patterning is purely based on size-dependent Nodal inhibition mediated by Lefty, providing a foundation for the proportionate allocation of all future tissues.

The scaling mechanism that we found crucially depends on the coupling of inhibitor concentration to embryo size, which is conferred by the high diffusivity of Lefty. Strikingly, a similar mechanism based on the coupling of cell volume to the concentration of a cell cycle inhibitor has recently been found to control cell size in yeast57. It is therefore possible that this simple mechanism might be widespread across various levels of biological organisation to coordinate growth with cellular functions and patterning.

Methods

Generating smaller embryos by extirpation

All procedures involving animals were executed in accordance with the guidelines of the State of Baden-Württemberg (Germany) and approved by the Regierungspräsidium Tübingen (35/9185.46-5, 35/9185.81-5).

Extirpation assays were performed using a glass capillary holder mounted on a Hamilton syringe and fixed in a micromanipulator (Narishige). Extirpations were performed in 4 hour post-fertilisation (hpf) pronase-dechorionated sphere stage embryos in Ringer's solution (116 mM NaCl, 2.8 mM KCl, 1 mM $CaCl_2$, 5 mM HEPES). To allow wound healing after extirpation, embryos were left undisturbed for 30 min at 28°C. The wound typically healed within 15 min after extirpation, and the extirpated embryos were then transferred to normal embryo medium. To assess the survival of extirpated embryos without considering other mechanical disruptions of the extirpation assay (such as wound healing failure or mechanical constraints due to changes in the embryo/yolk ratio), embryos that did not survive extirpation or that did not proceed to gastrulation were discarded.

For quantification of cell numbers, extirpated cells from pools of 10 embryos were transferred to individual PCR tubes containing 0.05% Trypsin solution (Gibco), and incubated for 15 min at 37°C. Dissociated cells were then quantified using a Neubauer chamber on an Olympus CKX41 microscope. Ten to 20 pools of extirpated cells from 10 embryos were quantified per extirpation experiment. The average number of extirpated cells per embryo was 820 ± 130 cells, which corresponds to ≈30% of the cells of an embryo at sphere stage with ≈3000 cells.

Whole-mount *in situ* hybridisation

fascin, *hgg1*, *vsx2*, *sox3*, *sox17*, and *sox32* RNA probes for *in situ* hybridisation assays were synthesised using SP6 or T7 polymerase (Roche) and DIG- (Roche) or DNP- (Perkin Elmer) modified ribonucleotides. RNA probes were purified by ethanol precipitation with 7.5 M lithium chloride. For chromogenic *in situs*, embryos were fixed overnight at 4°C in 4% formaldehyde and then processed using an In situ Pro hybridisation robot (Abimed/Intavis) and as previously described58 with the following modifications: no proteinase K treatment before 90% epiboly stage; no pre-absorption of the anti-DIG antibody (Roche, 11093274910); 5% dextran sulfate (Sigma) added to the hybridisation solution59; riboprobes were denatured at 80°C for 15 min and chilled on ice prior to hybridisation using a final concentration of 1-2 ng/µl.

For fluorescent *in situs* (FISH), the following modifications were used: the blocking solution contained 2% Blocking Reagent (Roche) in 1x MABTw; incubation with anti-DIG (Roche) or anti-DNP-POD (Perkin-Elmer, FP1129) antibodies at a dilution of 1:150 in blocking solution was carried out overnight with shaking at 4°C; after antibody incubation, embryos were washed six times for 20 to 30 min at room temperature with PBS containing 0.1% Tween (PBST), and the signal was developed with 100 µl of TSA Cy3 or Cy5 at a dilution of 1:75 in amplification buffer (Perkin Elmer) for 1 h at room temperature without shaking.

For imaging, embryos were embedded in 1% low-melting point agarose, transferred to glass bottom culture dishes (MatTek corporation), and oriented manually. Only embryos mounted with the vegetal-animal axis completely parallel to the cover glass were used for analysis. For chromogenic *in situ* samples, images were captured using an Axio Zoom.V16 (ZEISS). For fluorescent *in situ* samples, confocal laser scanning microscopy was performed using an LSM 780 NLO microscope (ZEISS). Images were processed using Fiji60. The number of *hgg1*, *sox17*, and *sox32*+ cells was quantified using the "multi-point selection" tool60. *fascin* and *sox3* expression domains44, 61 in the central-most embryo regions were quantified using the "measure" tool in Fiji. *fascin* was quantified from the margin of the embryo to the end of the domain with high expression values. *sox3* was quantified from the animal pole to the end of the domain with high expression values. The shield was excluded in the selection due to higher expression of mesendodermal markers in this region. The size of embryos (from the margin to the animal pole) was measured similarly using bright-field images.

Immunostaining

For immunostainings, anti-phospho-Histone H3 (Cell Signaling Technologies, 3377S) and anti-pSmad2/3 (Cell Signaling Technologies, 8828) antibodies were used.

Immunostaining for phospho-Histone H3 was carried out as described previously62 with a 1:500 dilution of the primary antibody. For pSmad2/3, specimens were incubated in cold acetone at -20°C for 20 min before blocking35. To ensure staining specificity, samples were exposed to low concentrations of anti-pSmad2/3 antibody (1:2000 or 1:5,000), and samples were washed for 24 h with PBST before adding the secondary antibody. The signal was then amplified using HRP-conjugated anti-rabbit antibodies (Jackson ImmunoResearch, 111-035-003) and TSA Cy3 or Cy5 at a dilution of 1:75 in amplification buffer (Perkin Elmer) for 45 min at room temperature without shaking. Embryos were mounted for imaging as described above for FISH, but with the dorsal-ventral axis parallel to the cover glass in the case of phospho-Histone H3 staining. Confocal laser scanning microscopy was performed using an LSM 780 NLO (ZEISS) confocal microscope, and images were processed using Fiji. The number of phospho-Histone H3-positive cells was quantified over a depth of 140 μm using the "find maxima" plug-in in Fiji, with a fixed noise tolerance of 10,000 and manual correction. pSmad2/3 distributions were quantified from the margin of the embryo to the end of pSmad2/3 nuclear staining using the "measure" tool in Fiji. Non-nuclear staining was excluded. The extent of pSmad2/3 signalling is variable along the embryonic margin, and the mean of the pSmad2/3 domain at 10 different points along the marginal zone is shown in all figures. The size of embryos from the margin to the animal pole was measured similarly using DAPI-stained images.

Cell density quantification

Cell density measurements were performed in untreated and extirpated H2A-GFP63 transgenic embryos. Embryos were mounted at 1 hpe and 2 hpe as described above for phospho-Histone H3 immunostaining. The number of cells was quantified as described above for pH3+ cells but over a depth of 80 μm. The automatic segmentation and assignment

of nuclei within the highly dense field of cells was carefully inspected visually and manually corrected.

Epiboly measurements

Untreated and extirpated embryos were imaged every 30 min after extirpation. Lateral images were taken. The extent of the embryo proper, the uncovered yolk, the blastoderm thickness, and the total length (embryo proper + yolk) were measured. To calculate the percentage of epiboly, the percentage of total length that was covered by the embryo proper was calculated. Blastoderm spreading during epiboly was calculated by subtracting the extent of the embryo proper at 1.5, 2, 3, and 4 hpe from the embryo proper extent at the first time point of analysis (1 hpe).

Light-sheet imaging for 3D reconstructions of *fascin* and pSmad2/3 domains

For 3D imaging, a Lightsheet Z.1 microscope (ZEISS) was used. Embryos were embedded in 1% low-melting point agarose and mounted in glass capillaries. For merging of the different views, far-red or green fluorescent beads (Thermo Fischer Scientific) were added to the agarose at a 1:200,000 dilution. After 3D reconstruction, 2D maps were generated as described previously64 and rotated to the correct perspective using Hugin panorama photo stitcher software (http://hugin.sourceforge.net).

To quantify the signal distribution in the resulting 2D maps, images were opened in Fiji and rotated by 90°. The region corresponding to the whole embryo was selected, and the average intensity of *fascin* or pSmad2/3 from every point of the embryonic vegetal-animal axis was obtained using the “plot profile” plug-in in Fiji. Distances in pixels were transformed into percentages of total embryo length with the vegetal-most side defined as 0% and the animal-most side as 100%. Intensity was then normalised by subtracting background values (i.e. the lowest intensity value closest to the animal pole of the embryo) and setting the highest intensity value to 1. For the quantification of pSmad2/3 distributions, background values were obtained by imaging *lefty* mRNA-injected embryos after pSmad2/3 immunostaining and normalised using the highest intensity value from the uninjected experimental data sets. 2D maps of DAPI were used as controls to rule out spatial inhomogeneities along the embryonic vegetal-animal axis. The graphs in Fig. 1e and Fig. 3b represent scaled average maps obtained from several embryos.

To re-dimensionalise the scaled 2D maps (Fig. 1g and Fig. 3d), distances were multiplied by the measured embryo diameter and divided by $\pi/2$. Intensities were averaged in bins of 2 μm, and the mean and standard error of different individuals were calculated piece-wise.

Assessment of Lefty1 and Lefty2 activity

mRNA encoding Lefty1- or Lefty2-GFP33 was generated by plasmid linearisation with NotI (NEB), purification with a Qiagen PCR clean-up kit, and *in vitro* transcription using SP6 mMessage mMachine kits (Ambion). Pronase-dechorionated wild type (TLAB) embryos at the one-cell stage were injected with different amounts of *lefty1-GFP* (22 pg, 43 pg, 86 pg) or *lefty2-GFP* (5 pg, 10 pg, 20 pg) mRNA along with 100 pg of 10 kDa Alexa546-dextran (Life Technologies). At sphere stage, three to five embryos per condition were imaged on an

LSM 780 (ZEISS) confocal laser scanning microscope, and eight embryos with three replicates per condition were collected for quantitative reverse transcription PCR (qRT-PCR) at 50% epiboly. Extracellular fluorescence intensity quantifications and qRT-PCR measurements with Promega Go-Taq qPCR Master Mix were executed as described previously33 using the zebrafish elongation factor *eF1α* as a normalisation control.

Immunoblotting

Wild type (TE) zebrafish embryos around 50% epiboly stage were deyolked manually with tweezers and a dissection needle. “Negative control” embryos were treated from 4- to 8-cell stages onward with the Nodal inhibitor SB-505124 (S4696; Sigma Aldrich) at 50 μM as described previously35. The efficiency of inhibitor treatment was confirmed by assessing the phenotypes of inhibitor-treated and DMSO-treated embryos at 24 hpf. “Positive control” embryos were injected with 10 pg Squint-encoding mRNA33 to induce endogenous *lefty1* expression, and staged according to the development of uninjected siblings. Deyolked embryo caps were transferred to microcentrifuge tubes, excess embryo medium was removed, embryos were mixed with sample buffer (94 mM Tris pH 6.8, 3% SDS, 15% glycerol, 150 mM DTT, 0.003% bromophenol blue; 1 μl per embryo), and lysed by vortexing and incubation at 95°C for 10 min. Before loading, the samples were vortexed again and cleared by brief centrifugation.

The Lefty1 and H3 signals originated from different SDS-polyacrylamide gels and PVDF membranes due to differences in the abundance and molecular weights of these proteins. For anti-Lefty1 western blots 5, 10, or 15 embryos were loaded on 10% SDS-polyacrylamide gels (5, 10, or 15 μl, respectively). Loading of samples at the concentration used for Lefty1 blots resulted in saturated H3 signal, and samples were therefore diluted five-fold to quantify H3 levels using 12% SDS-polyacrylamide gels. To resolve Lefty1 well and separate it from unspecific bands, we let proteins with a molecular weight of less than 25 kDa run off the gels for Lefty1 immunoblots, making subsequent detection of H3 (≈15 kDa) impossible.

Proteins were blotted onto PVDF membranes using the Trans-Blot Turbo Transfer System (Bio-Rad) in “mixed molecular weight” mode. Blotted membranes were blocked in PBST containing 5% milk powder for one hour at room temperature, and incubated with the primary antibody (diluted in PBST containing 5% milk powder; 1:2,000 for the Lefty1 antibody35, 1:10,000 for the Histone H3 antibody (Abcam, ab1791)) at 4°C overnight. The membranes were briefly rinsed with PBST, washed twice with PBST for 5 min, and washed two more times with PBST for 10 min at room temperature. Membranes were then incubated with HRP-coupled anti-rabbit antibody (Jackson ImmunoResearch, 111-035-003; diluted 1:10,000 in PBST containing 5% milk powder) for 1.5 h at room temperature, followed by a brief rinse with PBST, two washes with PBST for 5 min, and two washes for 10 min at room temperature. Fresh PBST was added to the membranes before application of SuperSignal West Dura Extended Duration Substrate (Thermo Fisher Scientific). Chemiluminescence was detected with a Fusion Solo (Vilber Lourmat) imaging system.

TIFF images were analysed in Fiji. Regions of interest (ROIs) were drawn around Lefty1 or H3 bands, and mean intensity values were used for further analysis. For lanes without clear Lefty1 bands, signal intensity was measured at the position of the expected molecular weight

based on embryos overexpressing *squint*. The ROI dimensions were constant for all lanes measured on a given membrane (Supplementary Fig. 8). We did not subtract background intensities for the quantifications in Supplementary Fig. 5, which appeared to be higher in untreated compared to extirpated embryos (Supplementary Fig. 8) although single bands in the untreated/extirpated samples did not consistently follow this general trend (perhaps representing yolk proteins65 and possibly reflecting sample-related differences in deyolking efficiency). Lefty1 signal from samples with 10 embryos provided the most reliable signal, whereas signal for samples with 5 embryos was not robustly detectable and signal from samples with 15 embryos might be close to saturation (Supplementary Fig. 5c).

Injection of *lefty1-GFP* mRNA into the YSL

mRNA encoding Lefty1-GFP33 was generated by plasmid linearisation with NotI-HF (NEB), purification with a Qiagen PCR clean-up kit, and *in vitro* transcription using SP6 mMessage mMachine kits (Ambion). To mimic endogenous Lefty secretion, a physiologically relevant amount of 100 pg of *lefty1-GFP* mRNA was precisely injected into 4 hpf (sphere stage) pronase-dechorionated embryos at two equidistant points (1 nl of 50 ng/µl *lefty1-GFP* mRNA per point) within the embryonic yolk syncytial layer (YSL). To identify physiologically relevant amounts, 40, 60, 80, 100, 160, and 200 pg of *lefty1-GFP* mRNA were tested in a careful titration series, and 100 pg of *lefty1-GFP* mRNA were found to most efficiently rescue *lefty1*$^{-/-}$;*lefty2*$^{-/-}$ mutants.

Extirpations were performed 20-30 min after YSL injections. Embryos were divided into three groups: one group was fixed at shield stage and processed for FISH, the second was incubated in embryo medium at 28°C in 24-well plates covered with 2% agarose (1 embryo per well) for phenotypic analysis at 24 hpf, and the third group was processed for imaging 45-60 min after YSL injections. Mounting for imaging was done as described above for FISH samples. Movies were recorded with identical imaging conditions. Embryos were imaged for a total of approximately 100 min, and Fiji was used to generate movies. For measurements of Lefty1-GFP intensity, injections of *lefty1-GFP* mRNA in the YSL and extirpations were performed as described above, but imaging was carried out 1.5-2 h after injection. Samples were captured with identical imaging conditions. 20 stacks were used for *z*-projections over a depth of 53 µm, and the intensity of equivalent areas of the images was quantified using the “measure” plug-in in Fiji.

Hindering Lefty1-GFP diffusion

The morphotrap construct40 comprises a strong GFP binder ($K_d \approx 0.3$ nM)66. The morphotrap construct was digested with XhoI and XbaI to insert the morphotrap into a *pCS2+* expression plasmid. mRNA was generated as described above for *lefty1-GFP*. 1 nl containing 100 - 150 pg mRNA encoding the morphotrap was injected into one-cell stage embryos for experiments shown in the middle panel of Supplementary Fig. 4e. Transplantation of cells expressing the morphotrap (bottom panel of Supplementary Fig. 4e) was performed as described above for extirpation experiments. Briefly, 50 - 100 cells were transplanted from a sphere stage donor previously injected with 200 pg morphotrap-encoding mRNA into sphere stage host embryos previously injected with 50 pg *lefty1-GFP* mRNA.

Time-lapse imaging experiments (Supplementary Movies 2 and 3) showed that Lefty1-GFP mobility from the YSL is strongly affected by the presence of the morphotrap. However, Lefty1-GFP mobility is not abolished entirely. This outcome is expected – even for a high-affinity GFP-binder – if binding is reversible and on/off-kinetics are fast39. The strong membrane localisation of Lefty1-GFP in embryos expressing the morphotrap confirmed the high affinity. The movement of the Lefty1-GFP signal appeared to follow the membranes in these embryos and is slow, consistent with a low fraction of mobile Lefty1-GFP. However, morphogenetic movements during epiboly might play an additional role in Lefty1-GFP transport, possibly facilitating Lefty spreading towards the animal pole.

Testing the effect of morphotrap binding on Lefty1-GFP activity

Wild type (TE) embryos were injected at the one-cell stage with 1 nl injection mix containing 5 or 30 pg *lefty1-GFP* mRNA and 0.05% phenol red. To test the effect of the morphotrap on Lefty1-GFP activity, 150 pg of *morphotrap* mRNA was included in the injection mix. Lefty overexpression phenotypes were evaluated at 24 hpf. Three groups of Nodal loss-of-function phenotypes were defined according to their strength (Supplementary Fig. 4f,g): mild (S1), intermediate (S2), and severe (S3). For imaging, embryos were mounted in 2% methylcellulose in embryo medium. Bright-field images were acquired with an Axio Zoom.V16 (ZEISS).

Lefty1-GFP gradient measurements

The physiologically relevant amount of 100 pg mRNA encoding Lefty1-GFP was injected into the YSL of *lefty1*$^{-/-}$;*lefty2*$^{-/-}$ embryos. One group of embryos was additionally injected with 150 pg of *morphotrap* mRNA at the one-cell stage. 90 min after YSL injections, embryos were mounted and imaged using an LSM 780 NLO (ZEISS) confocal laser scanning microscope. Embryos were imaged between 90-140 min after YSL injections. To measure gradients of secreted Lefty1-GFP from the YSL, maximum intensity projections were generated from 28 stacks over a depth of 194 μm, and the “plot profile” plug-in in Fiji was used to obtain the intensity of Lefty1-GFP from every point of the vegetal-animal axis in a central region of the embryo. Background values were obtained by imaging *lefty1*$^{-/-}$;*lefty2*$^{-/-}$ uninjected embryos (for the group injected with *lefty1-GFP* mRNA) or *lefty1*$^{-/-}$;*lefty2*$^{-/-}$ injected with morphotrap (for the group injected with *morphotrap* + *lefty1-GFP* mRNA).

Fluorescence Recovery After Photobleaching (FRAP)

Wild type (TE) embryos were injected at the one-cell stage with 1 nl injection mix containing 50 pg *lefty1-GFP* mRNA and 0.05% phenol red. In experiments where the effect of the morphotrap on Lefty1-GFP diffusivity was measured, 200 pg of mRNA encoding the morphotrap were included in the injection mix. Pronase-dechorionated embryos were selected for homogenous expression of the morphotrap using an Axio Zoom.V16 (ZEISS). Embryos were mounted around oblong to sphere stage in 1% low-melting agarose using 35 mm Glass Bottom Microwell Dishes (MatTek). FRAP was performed and analysed as described previously33, 67, 68 using an LSM 780 NLO (ZEISS) confocal microscope at an imaging depth of 30-40 μm. Diffusion coefficients and production rates were fitted to the recovery curves using previously published values for Lefty1-GFP protein stability33. The

fit was constrained with a minimal diffusion coefficient of 0.1 $\mu m^2/s$, which is on the order of the speed of cell movements during early zebrafish development33.

lefty1$^{-/-}$;*lefty2*$^{-/-}$ mutant rescue with the small-molecule Nodal inhibitor SB-505124

Rescue experiments were performed as recently described{Rogers, 2017 #2047}. Extirpations were performed in 4 hpf pronase-dechorionated embryos at sphere stage as described above. 30-40 min after extirpation, embryos were transferred to 24-well plates covered with 2% agarose (1 embryo per well) and treated with 4.8 μM SB-505124 in embryo medium starting 40 min after extirpation (≈30% epiboly stage). Embryos were then separated into two groups: one group was fixed 2-2.5 h after extirpation (shield stage) and processed for FISH, and the second group was further incubated with the inhibitor at 28°C until 24 hpf (20 h after extirpation) for phenotypic analysis. For the experiments with increasing Nodal inhibitor exposure, different concentrations from 6 to 12 μM SB-505124 in embryo medium were tested.

Mathematical modelling

Details of the computational screen and the parameters used for modelling of the size-dependent inhibition system are described in Supplementary Note 1 and Supplementary Table 2.

Code availability

The source code for custom scripts used for data analysis in this study is available from the corresponding author.

Statistics and reproducibility

Two tests were performed to assess whether experimental data was normally distributed: Kolmogorov-Smirnov (α=0.05) and Shapiro-Wilk tests (α=0.05). To check whether experimental groups were significantly different, two-sided Student's t-tests (α=0.05) were performed if the groups followed a normal distribution according to at least one of the tests. Mann-Whitney U tests (α=0.05) were performed if the groups did not follow a normal distribution.

Embryos from zebrafish crosses were randomly allocated into experimental groups for extirpation, injections, and drug treatments. Most experiments were carried out at least twice, and the findings of all key experiments were reliably reproduced. All replicates and precise p values are documented in the “Summary” sheet of Supplementary Table 1, which states the number of independent samples, embryos, and independent experiments.

Data availability

Supplementary Table 1 contains the source data for Fig. 1a/c/d/h, Fig. 2b/c/e-i, Fig. 3a, Fig. 5c-h, Fig. 6f-j, Fig. 7e, Supplementary Fig. 2a/b, Supplementary Fig. 3a-c, and Supplementary Fig. 4a-d. The data that support the findings of this study are available from the corresponding author on reasonable request.

Europe PMC Funders Author Manuscripts

Supplementary Material

Refer to Web version on PubMed Central for supplementary material.

Acknowledgements

We thank Caroline Hill for providing the Lefty1 antibody, Markus Affolter for providing the morphotrap construct, and Jelena Raspopovic and Nathan Lord for helpful comments. This work was supported by EMBO (M.A.C., L.M, P.M.) and HFSP (P.M.) long-term fellowships, the NSF Graduate Research Fellowship Program (K.W.R.), NIH grant GM56211 (A.F.S.), and funding from the Max Planck Society, ERC Starting Grant 637840, and HFSP Career Development Award CDA00031/2013-C (P.M).

References

1. Morgan TH. Half embryos and whole embryos from one of the first two blastomeres. Anatomischer Anzeiger. 1895; 10:623–685.
2. Cooke J. Control of somite number during morphogenesis of a vertebrate, *Xenopus laevis*. Nature. 1975; 254:196–199. [PubMed: 1113883]
3. Inomata H. Scaling of pattern formations and morphogen gradients. Development, growth & differentiation. 2017; 59:41–51.
4. Garcia M, Nahmad M, Reeves GT, Stathopoulos A. Size-dependent regulation of dorsal-ventral patterning in the early Drosophila embryo. Dev Biol. 2013; 381:286–299. [PubMed: 23800450]
5. Lauschke VM, Tsiairis CD, Francois P, Aulehla A. Scaling of embryonic patterning based on phase-gradient encoding. Nature. 2013; 493:101–105. [PubMed: 23254931]
6. Kicheva A, et al. Kinetics of morphogen gradient formation. Science. 2007; 315:521–525. [PubMed: 17255514]
7. Wartlick O, Kicheva A, González-Gaitán M. Morphogen gradient formation. Cold Spring Harbor Perspectives in Biology. 2009; 1:a001255–a001255. [PubMed: 20066104]
8. Yu SR, et al. Fgf8 morphogen gradient forms by a source-sink mechanism with freely diffusing molecules. Nature. 2009; 461:533–536. [PubMed: 19741606]
9. Rogers KW, Schier AF. Morphogen gradients: From generation to interpretation. Annual Review of Cell and Developmental Biology. 2011; 27:377–407.
10. Rogers KW, Müller P. Nodal and BMP dispersal during early zebrafish development. Dev Biol. 2018
11. Umulis DM, Othmer HG. Mechanisms of scaling in pattern formation. Development. 2013; 140:4830–4843. [PubMed: 24301464]
12. Gregor T, Bialek W, de Ruyter van Steveninck RR, Tank DW, Wieschaus EF. Diffusion and scaling during early embryonic pattern formation. Proc Natl Acad Sci U S A. 2005; 102:18403–18407. [PubMed: 16352710]
13. Gregor T, McGregor AP, Wieschaus EF. Shape and function of the Bicoid morphogen gradient in dipteran species with different sized embryos. Developmental Biology. 2008; 316:350–358. [PubMed: 18328473]
14. Ben-Zvi D, Shilo B-Z, Fainsod A, Barkai N. Scaling of the BMP activation gradient in Xenopus embryos. Nature. 2008; 453:1205–1211. [PubMed: 18580943]
15. Ben-Zvi D, Pyrowolakis G, Barkai N, Shilo BZ. Expansion-repression mechanism for scaling the Dpp activation gradient in *Drosophila* wing imaginal discs. Current Biology. 2011; 21:1391–1396. [PubMed: 21835621]
16. Hamaratoglu F, de Lachapelle AM, Pyrowolakis G, Bergmann S, Affolter M. Dpp signaling activity requires Pentagone to scale with tissue size in the growing *Drosophila* wing imaginal disc. PLoS Biol. 2011; 9:e1001182. [PubMed: 22039350]
17. Wartlick O, et al. Dynamics of Dpp signaling and proliferation control. Science. 2011; 331:1154–1159. [PubMed: 21385708]
18. Cheung D, Miles C, Kreitman M, Ma J. Scaling of the Bicoid morphogen gradient by a volume-dependent production rate. Development. 2011; 138:2741–2749. [PubMed: 21613328]

Europe PMC Funders Author Manuscripts

19. Wartlick O, Jülicher F, González-Gaitán M. Growth control by a moving morphogen gradient during *Drosophila* eye development. Development. 2014; 141:1884–1893. [PubMed: 24757005]
20. Kicheva A, et al. Coordination of progenitor specification and growth in mouse and chick spinal cord. Science. 2014; 345:1254927–1254927. [PubMed: 25258086]
21. Uygur A, et al. Scaling pattern to variations in size during development of the vertebrate neural tube. Dev Cell. 2016; 37:127–135. [PubMed: 27093082]
22. Schulte-Merker S, et al. Expression of zebrafish goosecoid and no tail gene products in wild-type and mutant no tail embryos. Development. 1994; 120:843–852. [PubMed: 7600961]
23. Schier AF. Nodal morphogens. Cold Spring Harbor Perspectives in Biology. 2009; 1:a003459–a003459. [PubMed: 20066122]
24. Chen C, Shen MM. Two modes by which Lefty proteins inhibit Nodal signaling. Current Biology. 2004; 14:618–624. [PubMed: 15062104]
25. Feldman B, et al. Zebrafish organizer development and germ-layer formation require nodal-related signals. Nature. 1998; 395:181–185. [PubMed: 9744277]
26. Rebagliati MR, Toyama R, Fricke C, Haffter P, Dawid IB. Zebrafish nodal-related genes are implicated in axial patterning and establishing left-right asymmetry. Developmental biology. 1998; 199:261–272. [PubMed: 9698446]
27. Sampath K, et al. Induction of the zebrafish ventral brain and floorplate requires cyclops/nodal signalling. Nature. 1998; 395:185–189. [PubMed: 9744278]
28. Meno C, et al. Mouse Lefty2 and zebrafish antivin are feedback inhibitors of nodal signaling during vertebrate gastrulation. Molecular Cell. 1999; 4:287–298. [PubMed: 10518210]
29. Feldman B, et al. Lefty antagonism of Squint is essential for normal gastrulation. Current Biology. 2002; 12:2129–2135. [PubMed: 12498688]
30. Chen Y, Schier AF. Lefty proteins are long-range inhibitors of squint-mediated nodal signaling. Current Biology. 2002; 12:2124–2128. [PubMed: 12498687]
31. Cheng SK, Olale F, Brivanlou AH, Schier AF. Lefty blocks a subset of TGFβ signals by antagonizing EGF-CFC coreceptors. PLoS Biology. 2004; 2:e30. [PubMed: 14966532]
32. Choi WY, Giraldez AJ, Schier AF. Target protectors reveal dampening and balancing of Nodal agonist and antagonist by miR-430. Science. 2007; 318:271–274. [PubMed: 17761850]
33. Müller P, et al. Differential diffusivity of Nodal and Lefty underlies a reaction-diffusion patterning system. Science. 2012; 336:721–724. [PubMed: 22499809]
34. Wang Y, Wang X, Wohland T, Sampath K. Extracellular interactions and ligand degradation shape the nodal morphogen gradient. Elife. 2016; 5:e13879. [PubMed: 27101364]
35. van Boxtel AL, et al. A temporal window for signal activation dictates the dimensions of a Nodal signaling domain. Developmental Cell. 2015; 35:175–185. [PubMed: 26506307]
36. Rogers KW, et al. Nodal patterning without Lefty inhibitory feedback is functional but fragile. Elife. 2017; 6:e28785. [PubMed: 29215332]
37. Xu C, et al. Nanog-like regulates endoderm formation through the Mxtx2-Nodal pathway. Dev Cell. 2012; 22:625–638. [PubMed: 22421047]
38. Marcon L, Diego X, Sharpe J, Müller P. High-throughput mathematical analysis identifies Turing networks for patterning with equally diffusing signals. eLife. 2016; 5:e14022. [PubMed: 27058171]
39. Müller P, Rogers KW, Yu SR, Brand M, Schier AF. Morphogen transport. Development. 2013; 140:1621–1638. [PubMed: 23533171]
40. Harmansa S, Hamaratoglu F, Affolter M, Caussinus E. Dpp spreading is required for medial but not for lateral wing disc growth. Nature. 2015; 527:317–322. [PubMed: 26550827]
41. Gritsman K, et al. The EGF-CFC protein one-eyed pinhead is essential for nodal signaling. Cell. 1999; 97:121–132. [PubMed: 10199408]
42. Mathieu J, et al. Nodal and Fgf pathways interact through a positive regulatory loop and synergize to maintain mesodermal cell populations. Development. 2004; 131:629–641. [PubMed: 14711879]
43. Bennett JT, et al. Nodal signaling activates differentiation genes during zebrafish gastrulation. Developmental Biology. 2007; 304:525–540. [PubMed: 17306247]

44. Liu Z, et al. Fscn1 is required for the trafficking of TGF-beta family type I receptors during endoderm formation. Nat Commun. 2016; 7 12603.
45. van Boxtel AL, Economou AD, Heliot C, Hill CS. Long-range signaling activation and local inhibition separate the mesoderm and endoderm lineages. Dev Cell. 2018; 44:179–191 e175. [PubMed: 29275993]
46. Dougan ST. The role of the zebrafish nodal-related genes squint and cyclops in patterning of mesendoderm. Development. 2003; 130:1837–1851. [PubMed: 12642489]
47. Pei W, Williams PH, Clark MD, Stemple DL, Feldman B. Environmental and genetic modifiers of squint penetrance during zebrafish embryogenesis. Developmental Biology. 2007; 308:368–378. [PubMed: 17583692]
48. Gierer A, Meinhardt H. A theory of biological pattern formation. Kybernetik. 1972; 12:30–39. [PubMed: 4663624]
49. Othmer HG, Pate E. Scale-invariance in reaction-diffusion models of spatial pattern formation. Proc Natl Acad Sci U S A. 1980; 77:4180–4184. [PubMed: 6933464]
50. Francois P, Vonica A, Brivanlou AH, Siggia ED. Scaling of BMP gradients in Xenopus embryos. Nature. 2009; 461:E1. discussion E2. [PubMed: 19736667]
51. Ben-Zvi D, Barkai N. Scaling of morphogen gradients by an expansion-repression integral feedback control. Proc Natl Acad Sci U S A. 2010; 107:6924–6929. [PubMed: 20356830]
52. Umulis DM. Analysis of dynamic morphogen scale invariance. Journal of the Royal Society, Interface. 2009; 6:1179–1191.
53. Inomata H, Shibata T, Haraguchi T, Sasai Y. Scaling of dorsal-ventral patterning by embryo size-dependent degradation of Spemann's organizer signals. Cell. 2013; 153:1296–1311. [PubMed: 23746842]
54. Ben-Zvi D, Fainsod A, Shilo BZ, Barkai N. Scaling of dorsal-ventral patterning in the Xenopus laevis embryo. Bioessays. 2014; 36:151–156. [PubMed: 24323952]
55. Werner S, et al. Scaling and regeneration of self-organized patterns. Physical review letters. 2015; 114:138101. [PubMed: 25884138]
56. Rasolonjanahary M, Vasiev B. Scaling of morphogenetic patterns in reaction-diffusion systems. J Theor Biol. 2016; 404:109–119. [PubMed: 27255960]
57. Schmoller KM, Turner JJ, Koivomagi M, Skotheim JM. Dilution of the cell cycle inhibitor Whi5 controls budding-yeast cell size. Nature. 2015; 526:268–272. [PubMed: 26390151]
58. Thisse C, Thisse B. High-resolution in situ hybridization to whole-mount zebrafish embryos. Nature Protocols. 2008; 3:59–69. [PubMed: 18193022]
59. Lauter G, Soll I, Hauptmann G. Two-color fluorescent in situ hybridization in the embryonic zebrafish brain using differential detection systems. BMC Dev Biol. 2011; 11:43. [PubMed: 21726453]
60. Schindelin J, et al. Fiji: an open-source platform for biological-image analysis. Nat Methods. 2012; 9:676–682. [PubMed: 22743772]
61. Dee CT, et al. A change in response to Bmp signalling precedes ectodermal fate choice. Int J Dev Biol. 2007; 51:79–84. [PubMed: 17183467]
62. Feng X, Adiarte EG, Devoto SH. Hedgehog acts directly on the zebrafish dermomyotome to promote myogenic differentiation. Dev Biol. 2006; 300:736–746. [PubMed: 17046741]
63. Pauls S, Geldmacher-Voss B, Campos-Ortega JA. A zebrafish histone variant H2A.F/Z and a transgenic H2A.F/Z:GFP fusion protein for in vivo studies of embryonic development. Development genes and evolution. 2001; 211:603–610. [PubMed: 11819118]
64. Schmid B, et al. High-speed panoramic light-sheet microscopy reveals global endodermal cell dynamics. Nat Commun. 2013; 4 2207.
65. Link V, Shevchenko A, Heisenberg CP. Proteomics of early zebrafish embryos. BMC Dev Biol. 2006; 6:1. [PubMed: 16412219]
66. Saerens D, et al. Identification of a universal VHH framework to graft non-canonical antigen-binding loops of camel single-domain antibodies. Journal of molecular biology. 2005
67. Pomreinke AP, et al. Dynamics of BMP signaling and distribution during zebrafish dorsal-ventral patterning. Elife. 2017; 6

68. Blässle A, et al. Quantitative diffusion measurements using the open-source software PyFRAP. Nat Commun. 2018; 9 1582.

Europe PMC Funders Author Manuscripts

Europe PMC Funders Author Manuscripts

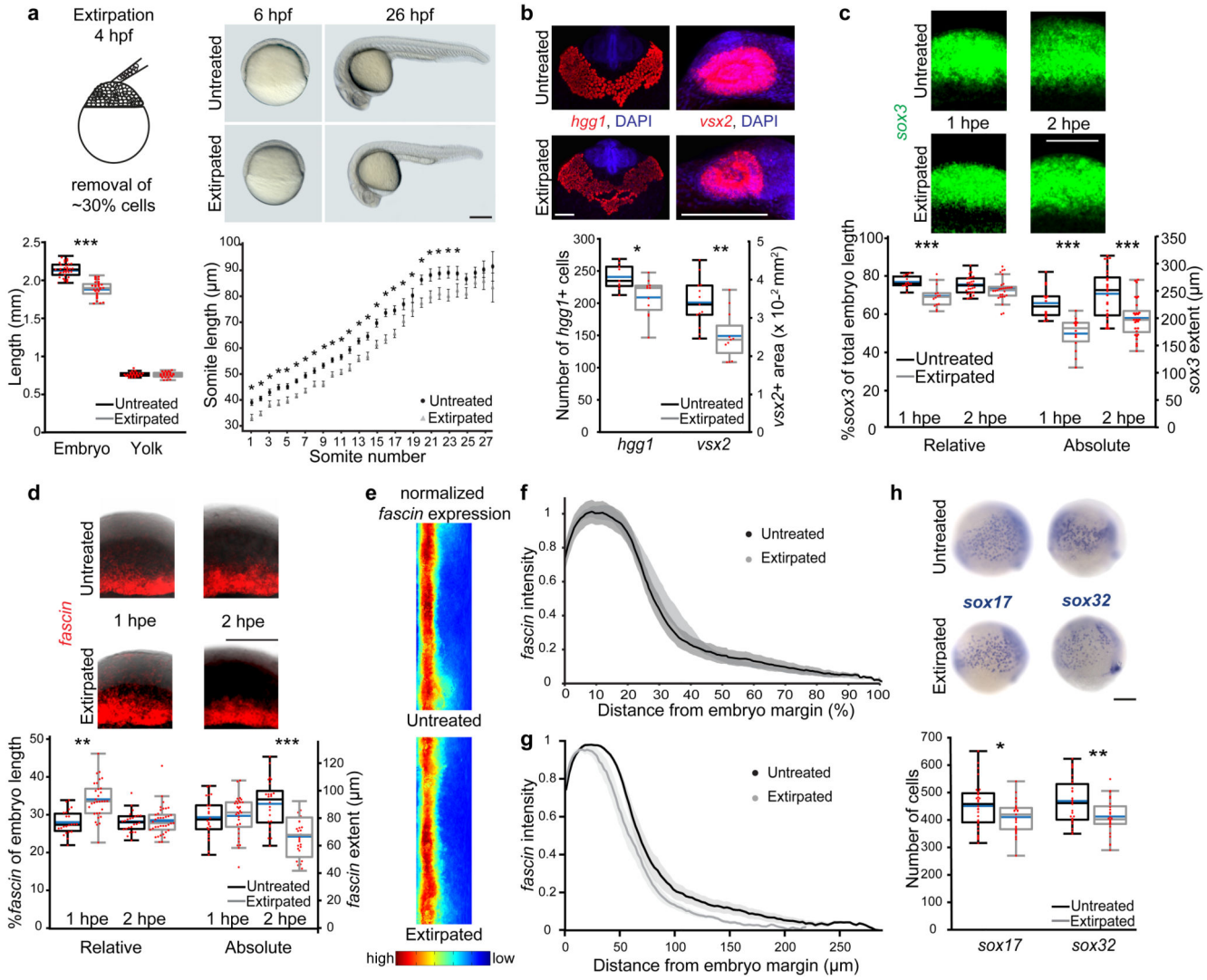

Figure 1. Scaling in smaller embryos after extirpation.

(a) Schematic of embryo extirpation; lateral views. The total length of extirpated embryos (grey bars) at 1 day post fertilisation is smaller than untreated individuals (black bars) (n[untreated]=40, n[extirpated]=37; ***p<0.00001), whereas yolk size remains unchanged (n[untreated]=23, n[extirpated]=24; p>0.05). The length of the 24 posterior-most somites is proportionately smaller in extirpated embryos (n[untreated]=15, n[extirpated]=13; *p<0.05). Error bars in “Somite length” graph: SEM. **(b)** Maximum intensity projections of confocal FISH stacks and quantification of *hgg1*- (n[untreated]=9, n[extirpated]=11; *p<0.05) and *vsx2*-positive cells (n[untreated]=13, n[extirpated]=11; **p<0.01). **(c,d)** Maximum intensity projections of lateral confocal FISH stacks, and quantification of the relative and absolute length of *sox3* (ectoderm) and *fascin* (mesendoderm) domains. Ectoderm proportions are smaller at 1 h post extirpation (hpe) (n[untreated]=14, n[extirpated]=14; ***p<0.001) but scale by 2 hpe (n[untreated]=28, n[extirpated]=28; p>0.05). Similarly, mesendoderm proportions are too large at 1 hpe (n[untreated]=23, n[extirpated]=31; **p<0.01) but scale by 2 hpe (n[untreated]=24, n[extirpated]=37; p>0.05). **(e-g)** 2D maps of 3D-reconstruced

embryos imaged by light-sheet microscopy, and quantification of normalised *fascin* domains along the vegetal-animal axis show scaling (n[untreated]=9, n[extirpated]=9). Shaded regions: SEM. **(h)** Lateral views and quantification of the number of endodermal cells positive for *sox17* (n[untreated]=30, n[extirpated]=27, *p<0.05) or *sox32* (n[untreated=26, n[extirpated]=28, **p<0.01). Box plots show median (blue line), mean (untreated: black, extirpated: grey lines inside the box), 25% quantiles (box) and all included data points (red markers). Whiskers extend to the smallest data point within the 1.5 interquartile range of the lower quartile, and to the largest data point within the 1.5 interquartile range of the upper quartile. Two-sided Student's t-tests were performed (α=0.05). See Supplementary Table 1 for statistics source data. Scale bars: 200 μm.

Europe PMC Funders Author Manuscripts

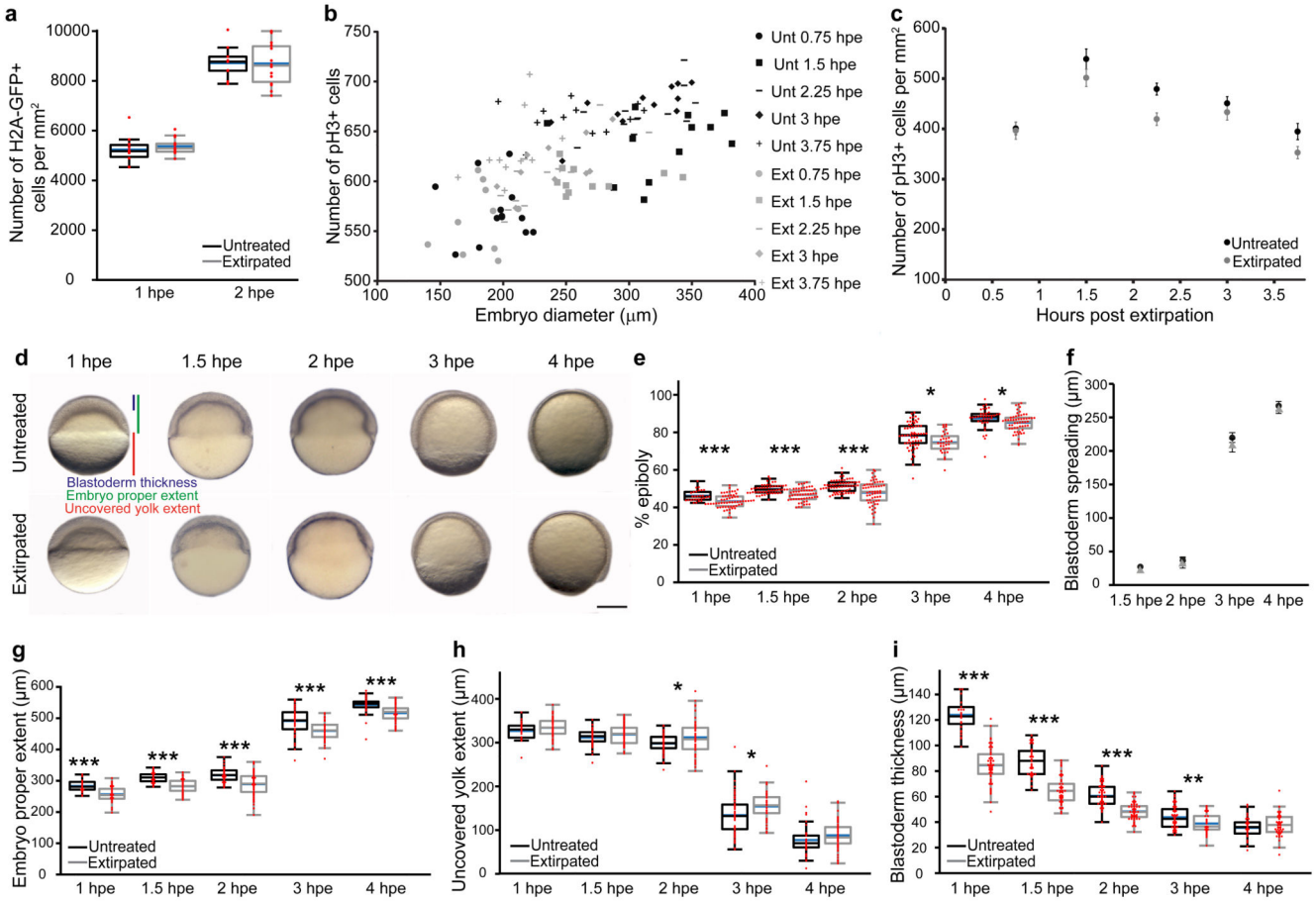

Figure 2. Germ layer proportions scale in extirpated embryos without increases in cell proliferation, or changes in cell density or developmental speed.

(a) Cell density measured in untreated and extirpated H2A-GFP embryos at different time points after extirpation. 1 hpe: n[untreated]=10, n[extirpated]=14, p>0.05; 2 hpe: n[untreated]=9, n[extirpated]=14, p>0.05. **(b,c)** Number of proliferating cells (phospho-Histone H3 (pH3) positive) relative to embryo diameter (b), and density of proliferating cells (c) in untreated and extirpated embryos at different time points after extirpation. 0.75 hpe: n[untreated]=13, n[extirpated]=11, p>0.05; 1.5 hpe: n[untreated]=12, n[extirpated]=11, p>0.05; 2.25 hpe: n[untreated]=12, n[extirpated]=12, **p<0.01; 3 hpe: n[untreated]=12, n[extirpated]=10, p>0.05; 3.75 hpe: n[untreated]=12, n[extirpated]=11, p>0.05. Individual data points are shown in (b); mean and SEM of the same data are shown in (c). **(d)** Lateral views of untreated and extirpated embryos. The progression of gastrulation and epiboly spreading is unchanged after extirpation. **(e-i)** Quantification of % epiboly ((e), i.e. the ratio of the embryo proper extent to the total length (embryo proper + uncovered yolk)), blastoderm spreading ((f), i.e. the difference between the embryo proper extent at 1.5, 2, 3, and 4 hpe and the embryo proper extent at the first time point of analysis (1 hpe)), extent of the embryo proper (g), uncovered yolk (h), and blastoderm thickness (i) at different time points after extirpation. 1 hpe: n[untreated]=28, n[extirpated]=59; 1.5 hpe: n[untreated]=51, n[extirpated]=55; 2 hpe: n[untreated]=62, n[extirpated]=58; 3 hpe: n[untreated]=59, n[extirpated]=33; 4 hpe: n[untreated]=38, n[extirpated]=55. *p<0.05; **p<0.01;

Europe PMC Funders Author Manuscripts

***p<0.001. Mean and SEM are shown in (f). Unt: Untreated; Ext: Extirpated. Box plot shows median (blue line), mean (untreated: black; extirpated: grey lines), 25% quantiles (box) and all included data points (red markers). Whiskers extend to the smallest data point within the 1.5 interquartile range of the lower quartile, and to the largest data point within the 1.5 interquartile range of the upper quartile. Two-sided Student's t-tests were performed (α=0.05). See Supplementary Table 1 for statistics source data.Scale bar: 200 μm.

Europe PMC Funders Author Manuscripts

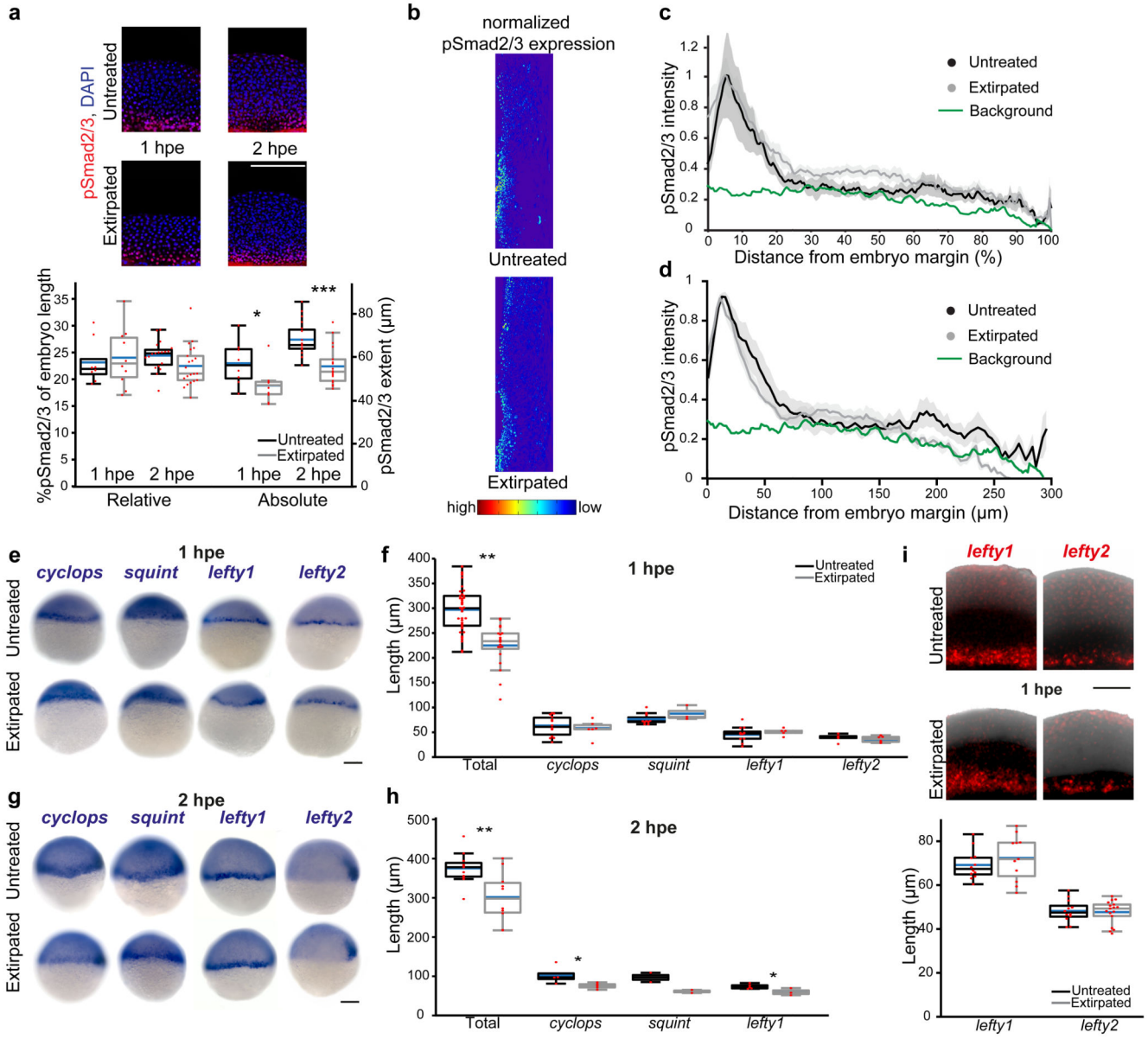

Figure 3. Scaling of Nodal-mediated patterning.

(a) Maximum intensity projections of lateral confocal pSmad2/3 immunostaining stacks, and quantification of the absolute and relative length of the pSmad2/3 domain. (1 hpe: n[untreated]=7, n[extirpated]=10; 2 hpe: n[untreated]=19, n[extirpated]=21; *p<0.05). **(b-d)** 2D maps of 3D-reconstruced embryos imaged by light-sheet microscopy, and quantification of normalised pSmad2/3 domains along the vegetal-animal axis show scaling (n[untreated]=5, n[extirpated]=6). (c) Intensity as a function of % embryo length; (d) intensity as a function of absolute distance from the margin. Shaded regions: SEM. **(e-h)** Lateral images showing the expression of *cyclops* and *squint* Nodals and *lefty1* and *lefty2* Leftys in untreated and extirpated embryos 1 (e) and 2 hpe (g), and quantification of embryo length and expression domains (f,h). 1 hpe: Total: n[untreated]=42, n[extirpated]=20; *cyclops*: n[untreated]=14, n[extirpated]=6; *squint*: n[untreated]=11, n[extirpated]=3; *lefty1*:

Europe PMC Funders Author Manuscripts

n[untreated]=12, n[extirpated]=5; *lefty2*: n[untreated]=5, n[extirpated]=6. 2 hpe: Total: n[untreated]=11, n[extirpated]=10; *cyclops*: n[untreated]=4, n[extirpated]=5; *squint*: n[untreated]=2, n[extirpated]=2; *lefty1*: n[untreated]=5, n[extirpated]=3. Nodal and Lefty domains are unchanged in differently sized embryos at 1 hpe, but scale by 2 hpe. **(i)** Maximum intensity projections of lateral confocal lefty1 and lefty2 FISH stacks in untreated and extirpated embryos at 1 hpe, and quantification of expression domains. *lefty1*: n[untreated]=12, n[extirpated]=11; *lefty2*: n[untreated]=12, n[extirpated]=17. Box plots show median (blue line), mean (untreated: black; extirpated: grey lines), 25% quantiles (box), and all included data points (red markers). Whiskers extend to the smallest data point within the 1.5 interquartile range of the lower quartile, and to the largest data point within the 1.5 interquartile range of the upper quartile. Two-sided Student's t-tests were performed (α=0.05). *p<0.05, **p<0.01, ***p<0.001. See Supplementary Table 1 for statistics source data. Scale bars: 200 μm and 100 μm (i).

Europe PMC Funders Author Manuscripts

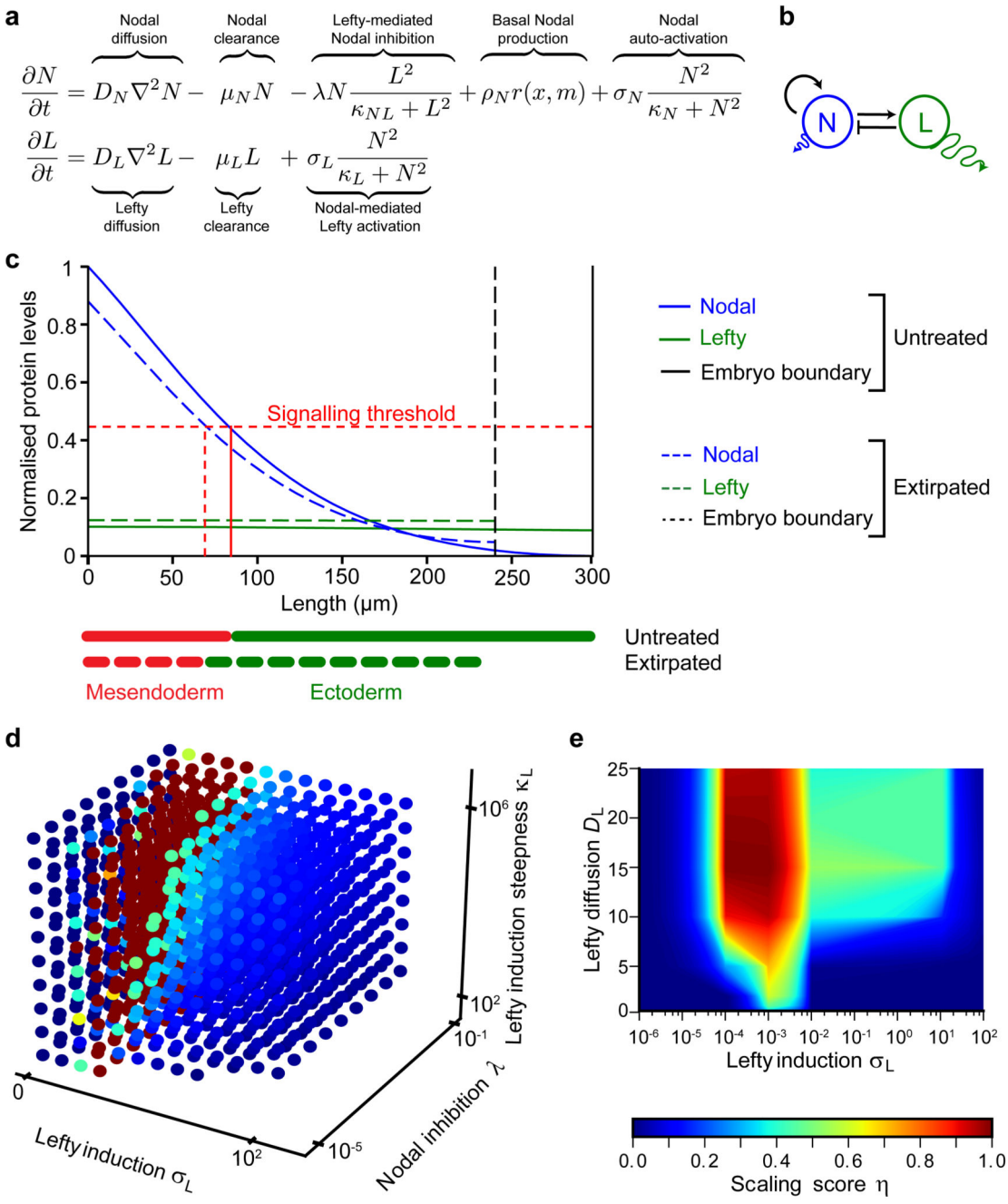

Figure 4. Computational screen for parameters conferring scale-invariance.

(a,b) Equations and network describing the known interactions in the Nodal/Lefty activator/inhibitor system. **(c)** Example of a scale-invariant system identified by the screen, showing an increase in Lefty and dampening of Nodal signalling after extirpation. Simulations were fitted to the experimentally measured total length and mesendoderm extent (Nodal signalling output). **(d)** Parameter screen showing the influence of Lefty levels (σ_L), Nodal inhibition strength (λ), and Lefty induction steepness (κ_L) on scaling; maximum projection through the six-dimensional parameter space with the following discrete values: for σ_L 0, 10^{-4}, 10^{-3},

10^{-2}, 11.12, 22.23, 33.34, 44.45, 55.56, 66.67, 77.78, 88.89, and 10^{2}; for λ 10^{-5}, $1.12 \cdot 10^{-2}$, $2.23 \cdot 10^{-2}$, $3.34 \cdot 10^{-2}$, $4.45 \cdot 10^{-2}$, $5.56 \cdot 10^{-2}$, $6.67 \cdot 10^{-2}$, $7.78 \cdot 10^{-2}$, $8.89 \cdot 10^{-2}$, and 10^{-1}; for κ_L 10^{2}, $1.12 \cdot 10^{5}$, $2.23 \cdot 10^{5}$, $3.34 \cdot 10^{5}$, $4.45 \cdot 10^{5}$, $5.56 \cdot 10^{5}$, $6.67 \cdot 10^{5}$, $7.78 \cdot 10^{5}$, $8.89 \cdot 10^{5}$, and 10^{6}. Parameter configurations resulting in biologically unrealistic gradients were excluded. **(e)** Parameter screen showing the influence of Lefty diffusivity on scaling; maximum projection through the six-dimensional parameter space. The model predicts that scaling should fail if Lefty induction or diffusion are too low (i.e. D_L less than ≈ 7 $\mu m^2/s$).

Europe PMC Funders Author Manuscripts

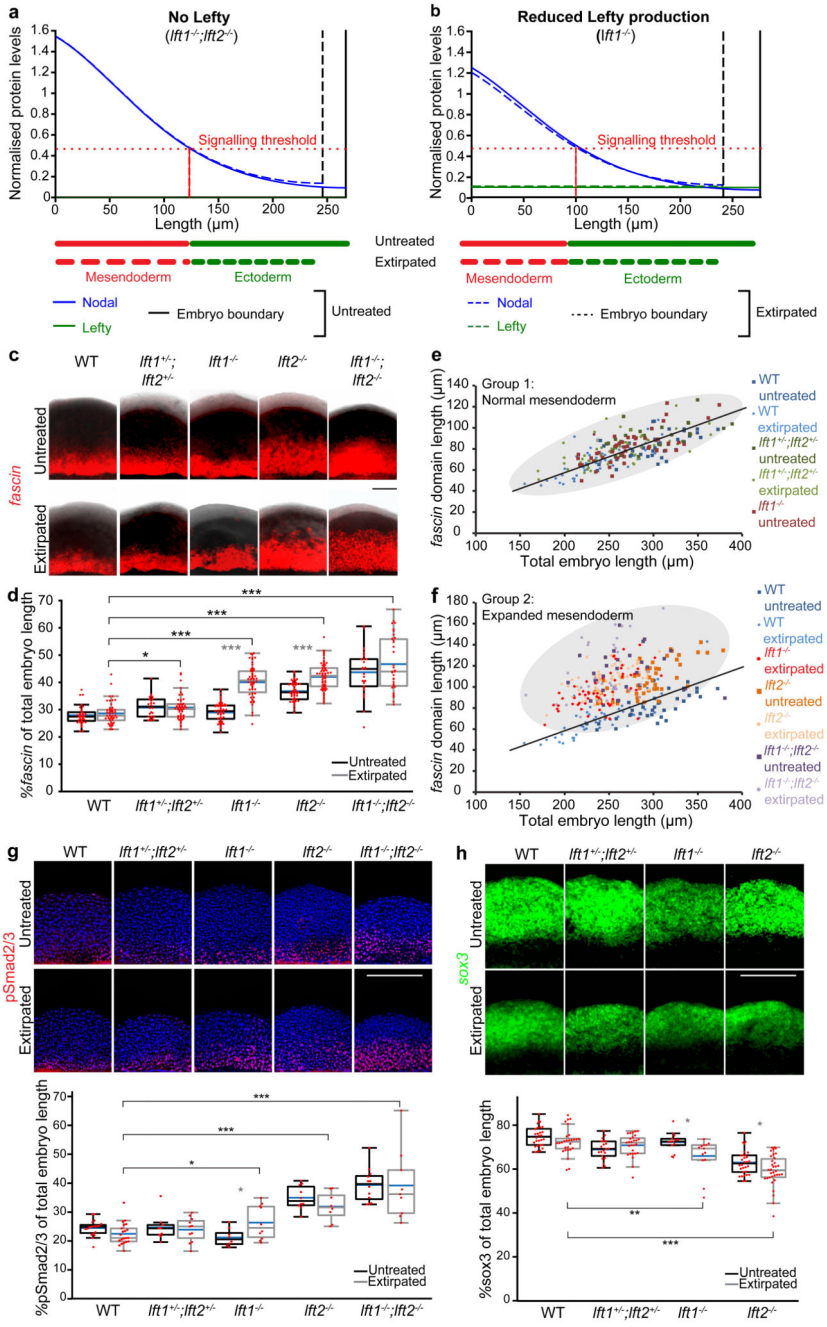

Figure 5. Germ layer scaling depends on Lefty levels.

(a,b) Simulations of the size-dependent inhibition predict that in the absence of Lefty mesendoderm is extended and does not scale (a), whereas reduced Lefty induction should prevent scaling in shortened embryos without a significant change in mesendoderm specification in normally sized individuals (b). **(c)** Maximum intensity projections of lateral confocal stacks of *fascin* FISH in untreated and extirpated embryos with different numbers of *lefty* alleles. **(d)** Quantification of *fascin*-positive mesendoderm proportions. The asterisks show differences between untreated and extirpated embryos (grey) and between WT and

lefty mutant extirpated embryos (black) (*p<0.05; **p<0.01; ***p<0.001). **(e,f)** Quantification of *fascin* relative to embryo length. The data for WT untreated and extirpated is plotted in both (e) and (f). For the *lefty* mutants, the encircled domains cluster two groups. Group 1 shows a similar mesendoderm proportion as WT individuals and a linear increase of mesendoderm with embryo size (e), whereas Group 2 clusters in a wider domain with larger mesendodermal proportions indicating absence of scaling. In c-f, WT: n[untreated]=38, n[extirpated]=49; *lft1*$^{+/-}$;*lft2*$^{+/-}$: n[untreated]=26, n[extirpated]=55; *lft1*$^{-/-}$: n[untreated]=50, n[extirpated]=58; *lft2*$^{-/-}$: n[untreated]=50, n[extirpated]=63; *lft1*$^{-/-}$;*lft2*$^{-/-}$: n[untreated]=29; n[extirpated]=34). **(g,h)** Maximum intensity projections of lateral confocal pSmad2/3 immunostaining (g) and *sox3* FISH (h) stacks, and quantification in 2 hpe embryos with different numbers of *lefty* alleles. For pSmad2/3: WT: n[untreated]=19, n[extirpated]=21; *lft1*$^{+/-}$;*lft2*$^{+/-}$: n[untreated]=10, n[extirpated]=11; *lft1*$^{-/-}$: n[untreated]=8, n[extirpated]=10; *lft2*$^{-/-}$: n[untreated]=9, n[extirpated]=8; *lft1*$^{-/-}$;*lft2*$^{-/-}$: n[untreated]=12; n[extirpated]=9. For *sox3*: WT: n[untreated]=28, n[extirpated]=28; *lft1*$^{+/-}$;*lft2*$^{+/-}$: n[untreated]=21, n[extirpated]=27; *lft1*$^{-/-}$: n[untreated]=14, n[extirpated]=13; *lft2*$^{-/-}$: n[untreated]=30, n[extirpated]=33. The asterisks show differences between untreated and extirpated (grey), and between extirpated WT and *lefty* mutant embryos (black) (*p<0.05; **p<0.01; ***p<0.001). Box plots show median (blue line), mean (untreated: black; extirpated: grey lines), 25% quantiles (box) and all included data points (red markers). Whiskers extend to the smallest data point within the 1.5 interquartile range of the lower quartile, and to the largest data point within the 1.5 interquartile range of the upper quartile. Two-sided Student's t-tests were performed (α=0.05). See Supplementary Table 1 for statistics source data. Scale bars: 70 μm (c) and 200 μm (g,h).

Europe PMC Funders Author Manuscripts

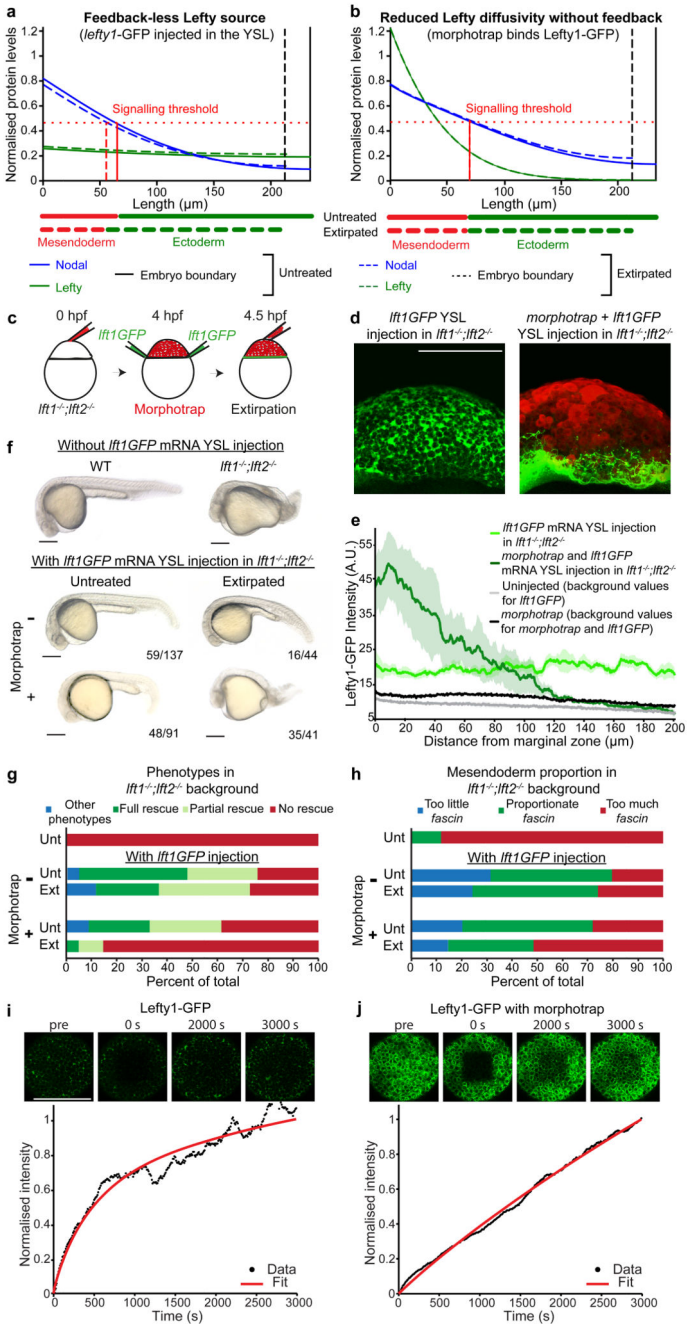

Figure 6. High Lefty diffusivity is required for scaling.

(a,b) Simulations of the model without feedback inhibition and hindered Lefty diffusion predict that a reduction in Lefty diffusivity – preventing Lefty from reaching the animal pole – should preclude scaling. **(c)** Schematic of morphotrap-mediated Lefty1-GFP diffusion hindrance in extirpated embryos. **(d)** Maximum intensity projections of confocal stacks of *lft1*$^{-/-}$;*lft2*$^{-/-}$ embryos injected with or without morphotrap (injected at the one-cell-stage) and *lefty1-GFP* mRNA in the YSL (injected at sphere stage). Lateral views. **(e)** Spatial distribution of Lefty1-GFP secreted from the YSL. The morphotrap prevents spreading of

Lefty1-GFP towards the animal pole of the embryo. n[*lefty1-GFP* mRNA injection]=6, n[*morphotrap*+*lefty1-GFP* mRNA injection]=3, n[background values]=1, n[background values morphotrap]=2. The experimentally determined distributions of Lefty1-GFP with morphotrap-mediated diffusion hindrance resemble the simulation of the "Reduced Lefty diffusivity" scenario (b). Shaded regions: SEM. **(f)** Lateral views of representative 26 hpf *lft1*$^{-/-}$;*lft2*$^{-/-}$ embryos with different treatments. Numbers in the figure panel indicate the fraction of these representative embryos. **(g)** Phenotype distributions in *lft1*$^{-/-}$;*lft2*$^{-/-}$ embryos after different treatments (n[*lft1*$^{-/-}$;*lft2*$^{-/-}$]=39; *lft1*$^{-/-}$;*lft2*$^{-/-}$+*lft1GFP*: n[untreated]=137, n[extirpated]=44; *lft1*$^{-/-}$;*lft2*$^{-/-}$+*morphotrap*+*lft1GFP*: n[untreated]=91, n[extirpated]=44). Embryos with partial rescue display imperfect tails and reduced cephalic structures (i.e. very mild Lefty-mutant phenotypes). **(h)** Fraction of treated *lft1*$^{-/-}$;*lft2*$^{-/-}$ embryos with low (<22%), normal (22-33%) and high (>34%) mesendoderm proportions (n[*lft1*$^{-/-}$;*lft2*$^{-/-}$]=44; *lft1*$^{-/-}$;*lft2*$^{-/-}$+*lft1GFP*: n[untreated]=67, n[extirpated]=66; *lft1*$^{-/-}$;*lft2*$^{-/-}$+*morphotrap*+*lft1GFP*: n[untreated]=35, n[extirpated]=37). The fraction of rescued and non-rescued *lft1*$^{-/-}$;*lft2*$^{-/-}$ embryos correlates with the fraction of normal and high mesendoderm proportions in (g) and (h). Unt: Untreated; Ext: Extirpated. **(i,j)** FRAP experiments demonstrate that Lefty1-GFP diffusion is hindered by the morphotrap. Representative FRAP data for Lefty1-GFP (i), and Lefty1-GFP with morphotrap (j). Microscopy images are shown before photobleaching (pre), immediately after (0 s), as well as 2000 s and 3000 s after photobleaching. Diffusion coefficients and production rates were fitted to the recovery curves using previously published values for Lefty1-GFP protein stability33. The mean diffusion coefficients were 7.7 ± 3.2 (SD) $\mu m^2/s$ for Lefty1-GFP (from n=6 independent experiments) and 0.2 ± 0.2 (SD) $\mu m^2/s$ for Lefty1-GFP with morphotrap (from n=4 independent experiments). See Supplementary Table 1 for statistics source data. Scale bars: 200 μm.

Europe PMC Funders Author Manuscripts

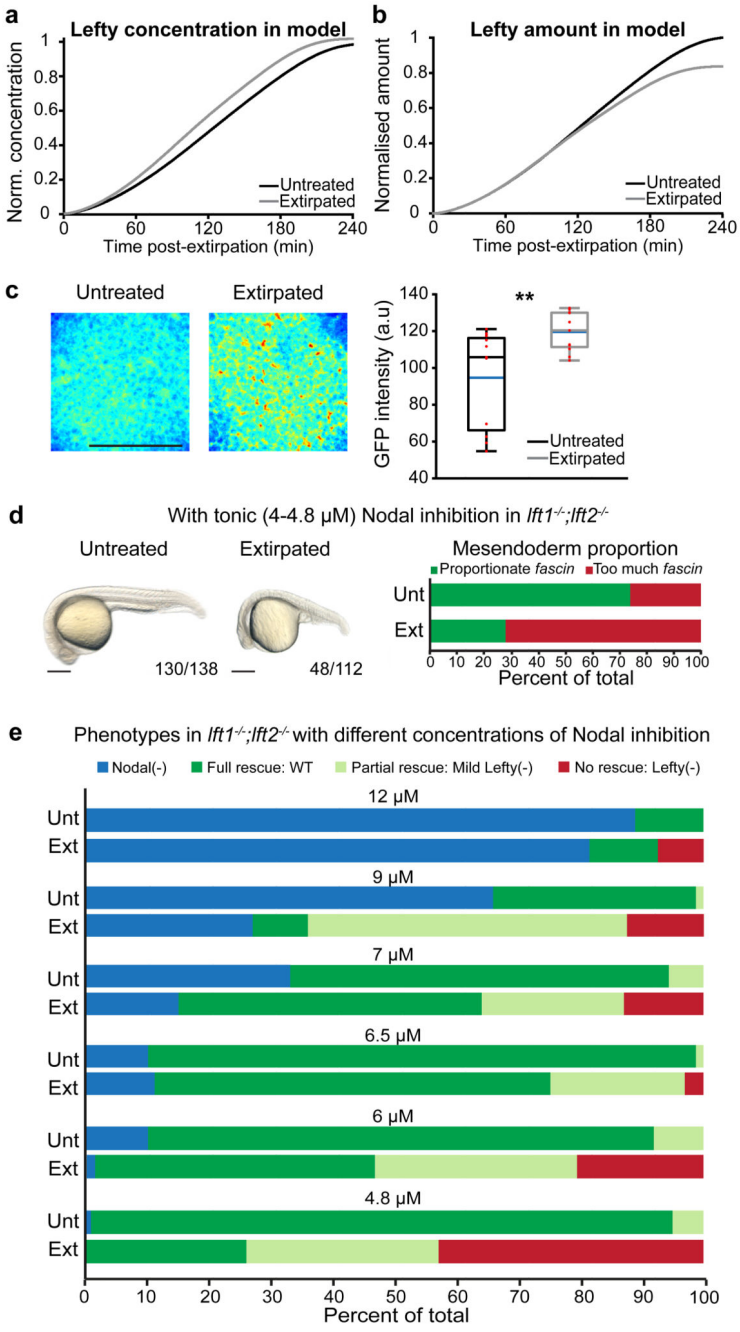

Figure 7. Lefty concentration increases in smaller embryos to allow scaling.

(a) Increase in Lefty concentration over time in smaller embryos predicted by the size-dependent inhibition model. **(b)** Decrease in Lefty amount over time in smaller embryos predicted by the size-dependent inhibition model. **(c)** Animal pole views of maximum intensity confocal stack projections of WT untreated and extirpated embryos injected with *lefty1-GFP* mRNA in the YSL, and quantification of GFP intensity; **p<0.01; n[untreated]=11, n[extirpated]=11. Box plot shows median (blue line), mean (untreated: black; extirpated: grey lines), 25% quantiles (box) and all included data points (red

markers). Whiskers extend to the smallest data point within the 1.5 interquartile range of lower quartile, and to the largest data point within the 1.5 interquartile range of the upper quartile. Two-sided Student's t-test were performed (α=0.05). **(d)** Lateral views of representative 26 hpf *lft1*$^{-/-}$;*lft2*$^{-/-}$ embryos exposed to 4-4.8 μM of the Nodal inhibitor SB-505124. Numbers in the figure panel indicate the fraction of these representative embryos. Mesendoderm quantification of *lft1*$^{-/-}$;*lft2*$^{-/-}$ embryos exposed to 4-4.8 μM of the Nodal inhibitor SB-505124 (n[untreated]=27, n[extirpated]=18). **(e)** Phenotype quantification in *lft1*$^{-/-}$;*lft2*$^{-/-}$ embryos exposed to different concentrations of the Nodal inhibitor SB-505124. Untreated: 4.8 μM n=138, 6 μM n=160, 6.5 μM n=80, 7 μM n=106, 9 μM n=85, 12 μM n=36; extirpated: 4.8 μM n=77, 6 μM n=146, 6.5 μM n=64, 7 μM n=108, 9 μM n=56, 12 μM n=27. Exposure to higher concentrations of the Nodal inhibitor SB-505124 increases *lft1*$^{-/-}$;*lft2*$^{-/-}$ mutant rescue after extirpation. The fraction of rescued and non-rescued *lft1*$^{-/-}$;*lft2*$^{-/-}$ embryos correlates with the fraction of normal and high mesendoderm proportions in (d). Unt: Untreated; Ext: Extirpated. See Supplementary Table 1 for statistics source data. Scale bars: 200 μm.